GPS/INS Integration for Estimation and Control During GPS Outages: A Cascaded Unscented Kalman Filters Approach

David Kun[a,*]

[a]*Neil Armstrong Hall of Engineering Rm. 3200A, 701 W. Stadium Ave., West Lafayette, IN 47907*

Abstract

Autonomous mobile systems require position measurements in order to maneuver and accomplish tasks. These measurements are usually obtained from Global Navigation Satellite Systems (e.g. GPS). However, at least four satellites need to be in view at all times, which may not be possible in environments with poor coverage due to buildings, tunnels, or radio frequency interference [6]. Receivers in these environments will be susceptible to GPS outages.

Various approaches to position estimation during GPS outages (e.g. using radio broadcasts from distance measuring equipment [17], using visual odometers [9], and employing simultaneous localization and mapping techniques [21]) rely on radio aids or adequate visibility, which might also be unavailable. An Inertial Navigation System (INS) integrates on-board sensor measurements independent of environmental conditions, but has rapidly growing error. By combining GPS and INS measurements, it is possible to improve INS error estimation and have a more reliable autonomous system during GPS outages.

This paper develops a cascaded estimation and control algorithm using two Unscented Kalman Filters (UKFs) for guiding a ground vehicle during short GPS outages. The results of several simulations show that this method provides significant improvement compared to previous methods that employ a single UKF or use two cascaded Extended Kalman Filters.

Keywords:
GPS-INS Integration, GPS Outages, Cascaded Kalman Filters, Unscented Kalman Filter

1. Introduction

Remotely-piloted and autonomous systems, such as unmanned aerial vehicles (UAVs) and autonomous land vehicles, require position measurements in order to accomplish most tasks and maneuvers. In most cases, the vehicles largely rely on Global Navigation Satellite Systems (GNSS), such as the Global Positioning System (GPS), for localization. The processed GPS signal is advantageous because it has time-independent error sources, and is characterized by long-term stability. Unfortunately, the vehicle must be able to receive at least four satellite signals at all times. This condition may not be satisfied in environments with physical obstructions or radio-frequency interference.

In order to compute position estimates during prolonged or frequent GPS outages, additional sensors are required, such as Inertial Measurement Units (IMUs), odometers, or vision-based sensors. Unfortunately, these sensors quickly accumulate error, or are not sufficiently accurate, when used alone.

Most attempts to overcome this difficulty involve one or both of the following approaches.

1. Fuse Inertial Navigation System (INS) and GPS measurements when GPS signals are available in order to better predict INS errors during GPS outages.
2. Use additional equipment (e.g. cameras) together with the INS in order to improve overall state estimates during GPS outages.

The algorithm in [5] fuses GPS and INS measurements in order to mitigate INS errors and enable relatively accurate estimation during GPS outages.

*Corresponding author
Email address: dkun@purdue.edu (David Kun)
URL: https://engineering.purdue.edu/HSL/ (David Kun)

Furthermore, the estimation filter is divided into two sub-filters, to prevent model errors from corrupting navigation states. The filters in [5], however, are Extended Kalman Filters (EKFs), which rely on a linear approximation of the system at each time step. To overcome this limitation, the UKF was developed in [14] and was applied to GPS/INS integration in [15].

In this paper, I extend the work done in [5] by implementing two Unscented Kalman Filters (UKFs) in a cascaded form. The use of cascaded UKFs for GPS/INS measurement fusion is a novel hybrid approach to the problem. It prevents vehicle model errors from affecting navigation errors (as a result of the cascaded architecture) and mitigates the errors induced by the Taylor linearization (by implementing UKFs instead of EKFs).

2. Literature Review

A common method for combining GPS and INS measurements relies on the use of the Kalman Filter (KF) or Extended Kalman Filter (EKF), as shown in the implementations of [5, 13, 19, 20]. The KF, which is valid only for linear systems, takes noisy measurements and produces the optimal estimate of unknown state variables. Since real systems are usually nonlinear, the EKF is used instead. The EKF linearizes the nonlinear state functions at each estimate by evaluating the Jacobian every time step, and then uses the original KF algorithm. In [13], the EKF is implemented in order to fuse IMU, odometer, and GPS data of a land vehicle, aided by two antennas' heading measurements. Normally, when the vehicle moves in a straight line at a constant speed, the heading and yaw rate gyro bias can become unobservable, which leads to large errors in position estimates. The two antennas, together with the odometer, are shown to overcome this problem, and reasonable position estimates are produced. In both [5] and [20], the authors use *two* Kalman Filters to achieve more accurate results. In [5], the state estimation is divided into two tasks, each using an EKF. This separation prevents errors in the vehicle model from corrupting the navigation states. In [20], a video camera and laser rangefinder (LRF) are added to a UAV for improved navigation capabilities. When GPS signals are available, the first KF is used to estimate the INS errors by fusing GPS/INS measurements, and the second KF is implemented simultaneously to correct the LRF and optic flow errors. During GPS outages, the INS errors are kept separate from the LRF and optic flow fused measurements, allowing for greater precision.

The authors in [19] take a slightly different approach to reduce the stand-alone INS error drift by computing the system dynamics-derived error estimates and using those to update the INS Kalman Filter. This approach relies on a very accurate system model, so the authors first use a fuzzy expert system identification method to derive an accurate system dynamics model. The position estimates are quite good for the land vehicle in their experiment, but the implementation is difficult and may not be as accurate with more complex systems such as UAVs.

Although the KF is a computationally efficient optimal estimator, the linearization required by the KF could produce unstable filters when there is overwhelming noise or when the system is highly nonlinear [14]. Additionally, deriving the necessary Jacobian matrices can be a difficult task. Instead, the authors in [14] develop an Unscented Kalman Filter (UKF), which uses deterministic sampling and statistical linearization rather than the typical Taylor series linearization. A UKF-based approach to fusing GPS/INS measurements is presented in [15]. The authors attempt to solve the GPS outage problem for unmanned helicopters, which experience substantial vibrations that corrupt readings of IMUs. The UKF outperforms the regular KF in such noisy and highly nonlinear systems. The authors fuse the GPS/INS measurements when the GPS signals are available, and successfully filter out most of the INS noise when GPS is not available.

Besides the UKF, an alternative way to avoid linearization is to use the Sequential Monte Carlo method, commonly known as a Particle Filter (PF). The PF implements Bayesian recursion equations for state estimation. It develops a Monte Carlo approximation of the state estimates using random particles, and does not require a linear model or any restrictions on noise in the system. The PF approach is implemented in [7, 8, 12]. The authors in [7] use a PF to fuse GPS and odometric measurements, and show that the PF is superior to the EKF during GPS outages. An interesting feature of this work is that the authors formulate an algorithm to make use of the available satellite signals when there are fewer than four in range. Using the PF to fuse two or three pseudoranges with the odometer measurements, they achieved much smaller estimation errors than with just the odometer measure-

ments.

As an improvement to the previous PF method, a hybrid filter is developed in [8], combining a PF with a Kalman Filter to fuse data from GPS, odometer, and digital road map measurements. The addition of the road map increases the accuracy of their model, but only in locations with digitally-mapped roads.

Although it may seem counterintuitive at first, the authors in [12] begin to tackle the INS error by removing some of the INS sensors. This reduced inertial sensor system (RISS) has only one single-axis gyroscope and one two-axis accelerometer. The RISS, together with an odometer, have fewer sensor errors than the standard INS. Next, the authors apply a variant of the PF, known as a Mixture Particle Filter. In a regular PF, the sampling/importance re-sampling PF samples from the prior importance density (the probabilistic system model), and the likelihood PF samples from the observation likelihood. Instead, the Mixture PF samples from both densities, achieves appropriate weighting, and the resamples. This Mixture PF leads to a better performance when compared to a regular PF or KF approach with a full INS.

Similar to the Particle Filter method, a Gaussian Process Regression (GPR) approach can be used as a nonlinear INS-errors predictor, which allows the EKF to better estimate all INS errors [2]. Another benefit of GPR is that it is model-independent, i.e. non-parametric. It simply creates a nonlinear probabilistic mapping from input space to output space. The predicted INS deviations are then fed to the KF, which performs a virtual update step to estimate and correct the INS errors. The authors ran extensive tests and were able to show that the GPR/EKF method for estimation outperformed the standard EKF method.

Instead of the aforementioned time domain-based filters, the authors in [11] implement a frequency-domain dynamic response method to model the INS/GPS system. The input to their dynamic system model is the INS-only solution, and the output is the INS/GPS integration solution. This process allows the derivation of the system transfer function, and thereby an estimate of the impulse response. During GPS outages, the convolution of the INS-only solution with the estimated impulse response is integrated numerically, to produce more accurate velocity and position estimates. The authors were able to show that this method provided more accurate position estimates than INS-only estimation.

A unique method to combine GPS and INS measurements is through the use of virtual satellites, nicknamed 'virtualites' [10].The authors in [10] take advantage of the existing GPS data processing software, and transform the INS measurements into virtual satellite measurements, such that the on-board GPS processing unit receives at least four signals (some real, some virtual). Therefore, no variant of the KF is required to process the INS and GPS measurements concurrently. Two virtualite methods were tried. The first method requires a single receiver to process real GPS signals alongside virtualite signals. The second method uses double-differenced virtual code measurements, which removed the need to simulate a receiver clock bias. The second method was more difficult to implement, but was more accurate than the first. Although the second method was a clear improvement, the errors were still quite significant relative to GPS-only measurements.

A more recent trend in approaching the GPS outage problem has been to use Artificial Intelligence to identify the INS error dynamics model. Some of the INS error comes from sensor inaccuracy, the rest is mostly from model inaccuracies. As a simple example, estimating a vehicle's position based on odometer measurements is highly dependent on knowledge of the diameter of the wheel (among other things). Similarly, inferences from sensor measurements require accurate error models. The authors in [16] use Wavelet Neural Network (WNN) algorithm to identify and model the INS errors. During GPS availability, the model is constructed and improved by the WNN algorithm. When GPS is unavailable, the new model is used with a strong tracking KF (STKF) for INS error compensation. There are numerous other AI-based methods, but the overarching principle is the same; apply an AI technique to 'learn' the INS error model when GPS is available, and use this knowledge to improve a filter (e.g. KF, PF, etc.) during GPS outages.

In general, all existing approaches have some evident disadvantages. Some require additional or more expensive equipment (e.g. [13, 20]); some require an odometer, which restricts the method to land-vehicles (e.g. [2, 7, 8, 12, 13]); and some replace the KF with a PF to avoid error biases, which generates computationally expensive algorithms (e.g. [7, 8, 12]).

3. Nomenclature

The following variable definitions are used in this paper:

E : tractor East position
N : tractor North position
V_x : forward velocity
ψ : heading
$\dot{\psi}$: yaw rate
$\ddot{\psi}$: yaw acceleration
δ : steer angle
$\dot{\delta}$: steering slew rate
ψ_b : heading bias
r_b : radar bias
g_b : gyroscope bias
δ_b : steer angle bias

4. Model Description

The simulations in this paper are based on a John Deere 8400 tractor. Its model dynamics were derived in [3], and a schematic of the vehicle is shown below (Figure 1).

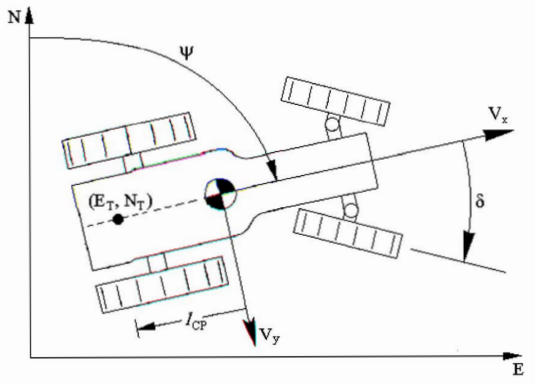

Figure 1: Free-Body Diagram [3]

The vehicle's position (East and North) is described by the following differential equations:

$$\dot{E} = V_x \sin(\psi) + \left(V_y - \dot{\psi} l_{CP}\right) \cos(\psi)$$
$$\dot{N} = V_x \cos(\psi) + \left(V_y - \dot{\psi} l_{CP}\right) \sin(\psi)$$

By placing the control point at the center of gravity, the distance $l_{CP} = 0$. Additionally, because $V_x \gg V_y$, the lateral velocity (V_y) due to vehicle sideslip is neglected, so $V_y \approx 0$. However, there may be a constant or slowly varying lateral velocity due to terrain or heading sensor misalignment. This is estimated as a heading bias in the Kalman filter. Then the new state equations become:

$$\dot{E} = V_x \sin(\psi) \tag{1}$$
$$\dot{N} = V_x \cos(\psi) \tag{2}$$

The vehicle's yaw dynamics from steer angle (δ) to yaw rate (ψ) are described by the following differential equation:

$$\dddot{\psi} = -2\zeta\omega_n \ddot{\psi} - \omega_n^2 \dot{\psi} + K_R \omega_n^2 \delta \tag{3}$$

where the DC gain (K_R), damping ratio (ζ), and natural frequency (ω_n) for the yaw dynamics are functions of velocity and were determined in [3] using system identification.

The steering valve dynamics from the control input (u) to steer angle (δ) are modeled as:

$$\ddot{\delta} = -\frac{1}{\tau_v}\dot{\delta} + \frac{K_v}{\tau_v} u \tag{4}$$

where the DC gain (K_v) and time constant (τ_v) for the steering dynamics were also determined in [3] using system identification.

The vehicle dynamics (Equations 1–4) are in the form:

$$\dot{X} = f(X) + Bu \tag{5}$$

where

$$X = \begin{bmatrix} E & N & V_x & \psi & \dot{\psi} & \ddot{\psi} & \delta & \dot{\delta} \end{bmatrix}^T \tag{6}$$

The 7th-order model must be augmented with four sensor biases ($r_b, g_b, \psi_b, \delta_b$) and a velocity ($V_x$) for an improved control architecture and full state feedback control. The resulting 12th-order state estimate vector is given by:

$$\hat{X} = \begin{bmatrix} \hat{E} & \hat{N} & \hat{r}_b & \hat{\psi} & \hat{g}_b & \hat{\psi}_b & \hat{\dot{\psi}} & \hat{\ddot{\psi}} & \hat{V}_x & \hat{\delta} & \hat{\dot{\delta}} & \hat{\delta}_b \end{bmatrix}^T \tag{7}$$

In Section 6, the state vector (Equation 7) will be divided into two parts, and two filters will be used for estimation.

The biases are assumed to be constant, but are modeled as first-order random walks in order to prevent the estimator gain from becoming zero. Four biases (steer angle δ_b, heading ψ_b, yaw gyroscope g_b, and radar r_b of 0.1, 0.2, 0.3, and 0.4, respectively) are added to each of the measurements.

The process noise and sensor noise variances are assumed to be uncorrelated with each other (such that the covariance matrices are diagonal) and are shown in Table 1 and Table 2, respectively[1].

Table 1: Process Noise Variances [5]

State	Variance (σ^2)	State	Variance (σ^2)
E	0.1 m^2	$\dot{\delta}$	0.01 $(\frac{rad}{s})^2$
N	0.1 m^2	V_x	0.01 $(\frac{rad}{s})^2$
ψ	0.01 rad^2	δ_b	10^{-3} rad^2
$\dot{\psi}$	0.1 $(\frac{rad}{s})^2$	g_b	10^{-3} $(\frac{rad}{s})^2$
$\ddot{\psi}$	0.1 $(\frac{rad}{s^2})^2$	r_b	10^{-3} $(\frac{m}{s})^2$
δ	0.01 rad^2	ψ_b	10^{-3} rad^2

Table 2: Sensor Noise Variances [5]

Measured State	Variance (σ^2)
E	$9.0 \times 10^{-4} m^2$
N	$9.0 \times 10^{-4} m^2$
ψ	$1.745 \times 10^{-3} rad^2$
$\dot{\psi}$	$6.0 \times 10^{-5} (rad/s)^2$
δ	$1.5 \times 10^{-3} (rad)^2$
V_x	$1.4 \times 10^{-2} (m/s)^2$

The sensors used for this study (in [3, 4, 5]) are: Real Time Kinematic (RTK) GPS for the East and North positions, Multi-Antenna GPS for the heading angle (ψ), Fiber Optic Gyroscope (FOG) for the yaw rate ($\dot{\psi}$), Linear Potentiometer for the steer angle (δ), and a Doppler Radar for the longitudinal velocity (V_x).

5. Control Algorithm

For straight line tracking, the desired heading angle (ψ_d) is constant. We can define a heading error as the difference between the estimated heading ($\hat{\psi}_d$) and the desired heading (ψ_d).

$$\hat{\psi}_{err} = \hat{\psi} - \psi_d \tag{8}$$

The lateral error ($\hat{y}_{err}$) of the vehicle is computed as the distance from the control point (at the CG) to the desired line.

$$\hat{y}_{err} = \left(\hat{E} - E_d\right)\cos(\psi_d) - \left(\hat{N} - N_d\right)\sin(\psi_d) \tag{9}$$

[1]Note that the steer angle rate ($\dot{\delta}$) variance was changed from 0.0 to 0.01, as it appears to be a typo in [5]. Also, all bias variances ($\delta_b, g_b, r_b, \psi_b$) were increased to 10^{-3} to make them more observable for both filters and improve their performance.

Given the fact that the desired heading angle is constant, $\dot{\hat{\psi}}_{err} = \dot{\hat{\psi}} - \dot{\psi}_d = \dot{\hat{\psi}}$. Similarly, $\ddot{\hat{\psi}}_{err} = \ddot{\hat{\psi}}$. Assuming small heading errors, we can define the lateral dynamics in a linearized form:

$$\dot{\hat{y}}_{err} = V_x \psi_{err} \tag{10}$$

Therefore, using Equations 3 and 4 and assuming constant desired velocity ($V_{x,d}$), we can construct a linear state-space form for the lateral control states (X_c):

$$A_c = \begin{bmatrix} 0 & V_{x,d} & 0 & 0 & 0 & 0 \\ 0 & 0 & 1 & 0 & 0 & 0 \\ 0 & 0 & 0 & 1 & 0 & 0 \\ 0 & 0 & -\omega_n^2 & -2\zeta\omega_n & K_R\omega_n^2 & 0 \\ 0 & 0 & 0 & 0 & 0 & 1 \\ 0 & 0 & 0 & 0 & 0 & -\frac{1}{\tau_v} \end{bmatrix}$$

$$B_c = \begin{bmatrix} 0 \\ 0 \\ 0 \\ 0 \\ 0 \\ \frac{K_v}{\tau_v} \end{bmatrix}, X_c = \begin{bmatrix} y_{err} \\ \psi_{err} \\ \dot{\psi} \\ \ddot{\psi} \\ \delta \\ \dot{\delta} \end{bmatrix}, \quad \dot{X}_c = A_c X_c + B_c u \tag{11}$$

Using the linearized system above, we can discretize it and compute the scalar input u by finding the Linear Quadratic Regulator (LQR) gains (K_c) and using:

$$u(k) = -K_c \hat{X}_c(k) \tag{12}$$

The LQR algorithm optimizes the cost function:

$$J_c = \sum_{k=0}^{\infty} X_c(k)^T Q_c X_c(k) + u(k)^T R_c u(k) \tag{13}$$

where,

$$Q_c = \text{diag}(\begin{bmatrix} 1 & 0 & 0 & 0 & 1 & 0 \end{bmatrix})$$
$$R_c = 0.1$$

The weighting matrix, Q_c, is chosen such that the lateral error is emphasized in the controller design. The second non-zero element in Q_c adds some damping to the steer angle (in order to avoid detrimental maneuvers).

A computationally efficient method to discretize a system like 11 is as follows:

$$\text{expm}\left(\begin{bmatrix} \mathbf{A} & \mathbf{B} \\ \mathbf{0} & \mathbf{0} \end{bmatrix} T_s\right) = \begin{bmatrix} \mathbf{A_d} & \mathbf{B_d} \\ \mathbf{0} & \mathbf{0} \end{bmatrix} \tag{14}$$

where *expm* is the matrix exponential, T_s is the sampling time, A_d and B_d are the discretized A and B matrix, respectively.

6. Cascaded State Estimation

Separating the estimation into two filters improves performance in several ways [5]. It allows more accurate estimation of the steer angle and gyroscope biases. In the single-system structure, an unknown bias in the steer angle sensor can create error in the yaw rate estimate, which in turn leads to an error in the gyroscope bias estimate. In the two-filter system, these cross-overs are not permissible. Also, the two-filter system allows one estimator to run at a higher frequency than the other, which can improve INS error estimation.

The first filter is the navigation estimator. Its states are given by:

$$X_1 = \begin{bmatrix} E & N & r_b & \psi & g_b & \psi_b \end{bmatrix}^T \tag{15}$$

By substituting the radar and gyroscope measurements (used as inputs) into Equations 1 and 3, we obtain:

$$\begin{aligned} \dot{E} &= \left(V_x^{radar} - r_b\right)\sin(\psi) \\ \dot{N} &= \left(V_x^{radar} - r_b\right)\cos(\psi) \\ \dot{\psi} &= \dot{\psi}^{gyro} - g_b \end{aligned} \tag{16}$$

These equations can be linearized about the desired heading (ψ_d) at each time step by evaluating the Jacobian matrix (J_1) and placing the equations in the following form:

$$\dot{X}_1 = J_1 X_1 + B_1 u_1 + w_1 \tag{17}$$

where,

$$J_1 = \begin{bmatrix} 0 & 0 & -\sin(\psi_d) & (V_x - r_b)\cos(\psi_d) & 0 & 0 \\ 0 & 0 & -\cos(\psi_d) & (V_x + r_b)\sin(\psi_d) & 0 & 0 \\ 0 & 0 & 0 & 0 & 0 & 0 \\ 0 & 0 & 0 & 0 & -1 & 0 \\ 0 & 0 & 0 & 0 & 0 & 0 \\ 0 & 0 & 0 & 0 & 0 & 0 \end{bmatrix}$$

$$X_1 = \begin{bmatrix} E \\ N \\ r_b \\ \psi \\ g_b \\ \psi_b \end{bmatrix}, B_1 = \begin{bmatrix} \sin(\psi_d) & 0 \\ \cos(\psi_d) & 0 \\ 0 & 0 \\ 0 & 1 \\ 0 & 0 \\ 0 & 0 \end{bmatrix}, u_1 = \begin{bmatrix} V_x^{radar} \\ \dot{\psi}^{gyro} \end{bmatrix}$$

where w_1 is a random process noise vector defined by the covariances in Table 1.

The second filter is the control estimator. Its states are given by:

$$X_2 = \begin{bmatrix} \dot{\psi} & \ddot{\psi} & V_x & \delta & \dot{\delta} & \delta_b \end{bmatrix}^T \tag{18}$$

From the yaw dynamics (Equation 3) and steering dynamics (Equation 4), which are already linear, we can place the control states directly into the form:

$$\dot{X}_2 = J_2 X_2 + B_2 u + w_2 \tag{19}$$

where,

$$J_2 = \begin{bmatrix} 0 & 1 & 0 & 0 & 0 & 0 \\ -\omega_n^2 & -2\zeta\omega_n & 0 & K_R\omega_n & 0 & 0 \\ 0 & 0 & 0 & 0 & 0 & 0 \\ 0 & 0 & 0 & 0 & 1 & 0 \\ 0 & 0 & 0 & 0 & -\frac{1}{\tau_v} & 0 \\ 0 & 0 & 0 & 0 & 0 & 0 \end{bmatrix}$$

$$X_2 = \begin{bmatrix} \dot{\psi} \\ \ddot{\psi} \\ V_x \\ \delta \\ \dot{\delta} \\ \delta_b \end{bmatrix}, B_2 = \begin{bmatrix} 0 \\ 0 \\ 0 \\ 0 \\ \frac{K_v}{\tau_v} \\ 0 \end{bmatrix}, u = -K_c\hat{X}_c$$

where w_2 is a random process noise vector defined by the covariances in Table 1.

The observations for each subsystems are described by:

$$Y_1 = C_1 X_1 + v_1 \qquad Y_2 = C_2 X_2 + v_2$$

where,

$$Y_1 = \begin{bmatrix} E^{GPS} & N^{GPS} & \psi^{GPS} \end{bmatrix}$$

$$Y_2 = \begin{bmatrix} \psi^{meas} & V^{meas} & \delta^{pot} \end{bmatrix}$$

$$C_1 = \begin{bmatrix} 1 & 0 & 0 & 0 & 0 & 0 \\ 0 & 1 & 0 & 0 & 0 & 0 \\ 0 & 0 & 0 & 1 & 0 & 1 \end{bmatrix}$$

$$C_2 = \begin{bmatrix} 1 & 0 & 0 & 0 & 0 & 0 \\ 0 & 0 & 1 & 0 & 0 & 0 \\ 0 & 0 & 0 & 1 & 0 & 1 \end{bmatrix}$$

and v_1 and v_2 are random sensor noise vectors defined by the covariances in Table 2.

Note that $C_1 = \mathbf{0}_{(3\times 6)}$ when GPS signals are not available, so the Kalman gain (L_1) becomes zero and the measurement values of Y_1 will have no effect on the estimation in the first filter during GPS outages.

In summary, the first filter estimates INS biases while GPS is available, so it provides more accurate positioning during GPS outages. The second filter uses the corrected INS measurements alongside steer angle measurements for controlling the vehicle.

Two types of estimation techniques (EKF and UKF) will be used on these cascaded subsystems for comparison. The EKF (which was used in [5]) is explained in Section 7 and the UKF is explained in Section 8.

7. Extended Kalman Filter

The Extended Kalman Filter (EKF) is based on the original KF, but applies to nonlinear systems. It is widely used in navigation systems with GPS applications. The general system has the form:

$$\begin{aligned} x_{k+1} &= f(x_k, u_{k+1}) + w_k \\ y_k &= h(x_k) + v_k \end{aligned} \tag{20}$$

where x, y are the state and measurement vectors respectively, $f(\cdot), g(\cdot)$ are continuous functions, and w, v are the process and sensor noise vectors respectively.

The EKF algorithm involves a measurement update followed by a time update, which are performed at each time step (k). The measurement update is given by:

$$\begin{aligned} L_k &= P_k^- C^T \left(CP_k^- C^T + R\right)^{-1} \\ \hat{X}_k^+ &= \hat{X}_k^- + L_k(Y_k - C\hat{X}_k^-) \\ P_k^+ &= (I - L_k C)P_k^- \end{aligned} \tag{21}$$

where,

L : Kalman gain vector
P : Estimated error covariance matrix
C : Observation matrix
R : Sensor noise covariance matrix
$\hat{X}_k^+$: Estimated state vector $\hat{X}(k|k)$
$\hat{X}_k^-$: Estimated state vector $\hat{X}(k|k-1)$
Y : Measurement vector $Y_k = CX_k + v_k$
I : Identity matrix

The time update is implemented by using Euler integration as shown below:

$$\begin{aligned} \hat{X}_{k+1}^- &= \hat{X}_k^+ + T_s \dot{X}_k \\ P_{k+1}^- &= \Phi_k P_k^+ \Phi_k^T + Q \end{aligned} \tag{22}$$

where,

T_s : Sampling time
$\dot{X}$: Calculated from nonlinear (1)-(4)
Φ : Discretized Jacobian
Q : Discretized process noise covariance matrix

The navigation filter (filter 1) uses Equations (21) and (22) for estimation. The control filter (filter 2) also uses the measurement update (21), but since it is a linear filter, the time update can be computed by:

$$\begin{aligned} \hat{X}_{k+1}^- &= \Phi_k \hat{X}_k^+ + \Gamma u_k \\ P_{k+1}^- &= \Phi_k P_k^+ \Phi_k^T + Q \end{aligned} \tag{23}$$

where,

Φ : Discretized Jacobian (J_2)
Γ : Discretized input matrix (B_2)
Q : Discretized process noise covariance matrix

The sensor noise covariance matrix (R) is a diagonal matrix composed of the variances in Table 2, and the process noise covariance matrix (Q) is a diagonal matrix composed of the variances in Table 1.

8. Unscented Kalman Filter

The Unscented Kalman Filter (UKF) was developed in [14] to overcome some of the limitations of the EKF. The new algorithm has two principle advantages over the EKF. First, it predicts the system state more accurately by avoiding linearization of the system. Second, it is simpler to implement. The UKF algorithm involves a calculation of sigma-points based on state covariance, followed by a time update, and a measurement update that are performed at each time step (k). The following algorithm is applicable to the general system shown in Equation (20).

The sigma vectors (χ) are used to propagate a random vector through a nonlinear function, and are formulated as follows:

$$\begin{aligned} \chi_0 &= \bar{X} \\ \chi_i &= \bar{X} + \left(\sqrt{(L+\lambda)P_x}\right)_i, \quad i = 1, ..., L \\ \chi_i &= \bar{X} - \left(\sqrt{(L+\lambda)P_x}\right)_{i-L}, \quad i = L+1, ..., 2L \end{aligned} \tag{24}$$

where X is the random state vector of dimension L, with mean $\bar{X}$ and covariance P_x. χ is the sigma vector of dimension $2L+1$. And $\lambda = \alpha^2(L+\kappa) - L$ is a scaling parameter, with $\alpha = 10^{-3}, \kappa = 0, \beta = 2$ as the default tuning parameters.

The corresponding weight vectors $(W^{(c)}, W^{(m)})$ are formulated as follows:

$$
\begin{aligned}
W_0^{(m)} &= \frac{\lambda}{(L+\lambda)} \\
W_0^{(c)} &= \frac{\lambda}{(L+\lambda)} + (1-\alpha^2+\beta) \\
W_i^{(m)} &= W_i^{(c)} = \frac{1}{2(L+\lambda)}, \quad i = 1, ..., 2L
\end{aligned} \tag{25}
$$

The time update equation is given by:

$$
\begin{aligned}
\chi^x_{k|k-1} &= f(\chi^x_{k-1}, \chi^v_{k-1}) \\
\hat{x}_k^- &= \sum_{i=0}^{2L} W_i^{(m)} \chi^x_{i,k|k-1} \\
P_k^- &= \sum_{i=0}^{2L} W_i^{(c)} \left[\chi^x_{i,k|k-1} - \hat{x}_k^-\right] \left[\chi^x_{i,k|k-1} - \hat{x}_k^-\right]^T \\
Y_{k|k-1} &= h(\chi^x_{k|k-1}, \chi^n_{k-1}) \\
\hat{y}_k^- &= \sum_{i=0}^{2L} W_i^{(m)} Y_{i,k|k-1}
\end{aligned} \tag{26}
$$

The measurement update equation is given by:

$$
\begin{aligned}
P_y &= \sum_{i=0}^{2L} W_i^{(c)} \left[Y_{i,k|k-1} - \hat{y}_k^-\right] \left[Y_{i,k|k-1} - \hat{y}_k^-\right]^T \\
P_{xy} &= \sum_{i=0}^{2L} W_i^{(c)} \left[\chi_{i,k|k-1} - \hat{x}_k^-\right] \left[Y_{i,k|k-1} - \hat{y}_k^-\right]^T \\
K &= P_{xy} P_y^{-1} \\
\hat{x}_k &= \hat{x}_k^- + K(y_k - \hat{y}_k^-) \\
P_k &= P_k^- - K P_y K^T
\end{aligned} \tag{27}
$$

The following section compares the performance of the EKF and UKF for estimating the states and biases with various types of disturbances and step inputs.

9. Simulation Results

The plots in this section highlight the performance of the two types of Kalman Filter as they integrate INS and (simulated) GPS measurements in order to estimate the biases of the on-board sensors. The EKF results will be presented first, followed by UKF results. Finally, this section concludes with a comparison of their performance.

The states of the subsystems were initialized as:

$$
X_1(0) = \begin{bmatrix} 0 \\ 0 \\ r_b \\ \psi_d \\ g_b \\ \psi_b \end{bmatrix}, \; X_2(0) = \begin{bmatrix} 0 \\ 0 \\ V_{x,d} \\ 0 \\ 0 \\ \delta_b \end{bmatrix}
$$

$$
\hat{X}_1(0) = \hat{X}_2(0) = \text{zeros}(6, 1)
$$

The simulations were run at 50 Hz (i.e. $T_s = 0.02$ sec) for 80 seconds with a velocity of $V_{x,d} = 3$ m/s, which has the corresponding constant parameters shown in Table 3.

Table 3: Parameters for $V_x = 3.0$ m/s

Parameter	Value
K_R	1.0
ζ	0.35
ω_n	6.4 rad/s
K_v	1.0
τ_v	0.1053 s

These parameters were found from best-fit lines of empirical results in [4]. The desired heading angle (ψ_d) is 0 degrees (i.e. due North).

In all of the following results, the tractor is using automatic steering control for straight line tracking (as explained in Section 5). A lateral step input of 3 meters (due East) was provided (as shown in Figure 2) as an initial perturbation to verify the control and estimation.

9.1. Extended Kalman Filter Results

An 'aerial' view of the vehicle's trajectory is shown in Figure 2, together with a plot of the East estimation error of the Extended Kalman Filter. The initial, larger error is partly due to transient behavior of the estimator and partly due to the vehicle's initial maneuver.

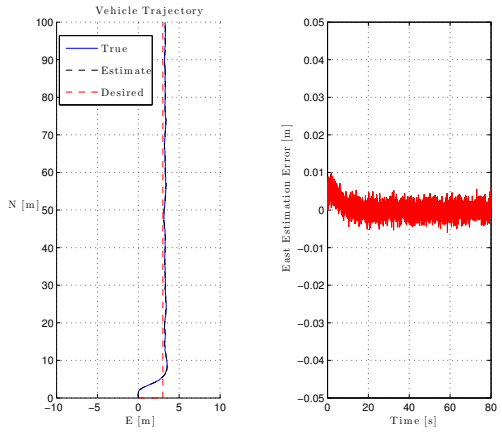

Figure 2: Straight Line Tracking & Position Error

The estimations of the four biases are shown in Figure 3. The radar, gyroscope, and heading bias are estimated by the first (navigation) filter. The steer bias is estimated by the second (control) filter. The radar bias estimate takes roughly twice as long to converge to a reasonable approximation, as compared to the other bias estimates.

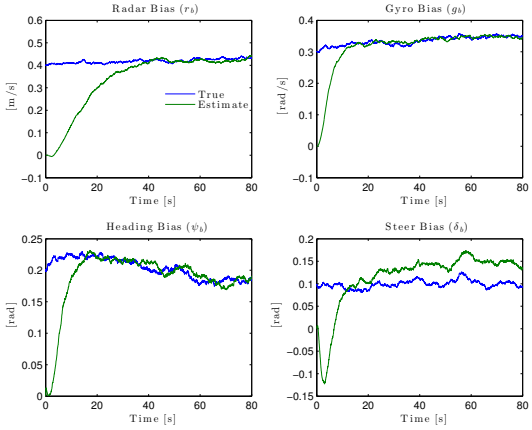

Figure 3: Bias Estimation during Straight Line Tracking

Figure 4 and Figure 5 display the gyroscope and radar measurements, respectively. These simulated measurements oscillate about their respective biases. The estimator converges to the biases in approximately 20 seconds.

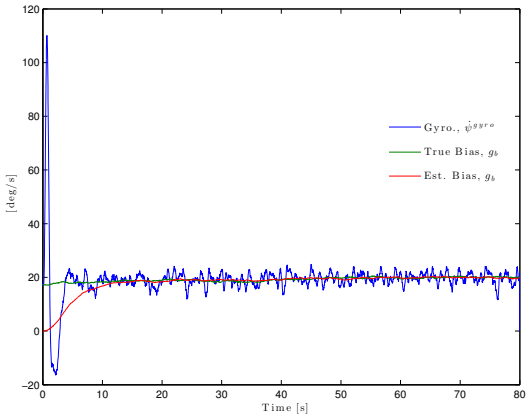

Figure 4: Gyroscope Measurements and Bias during Straight Line Tracking

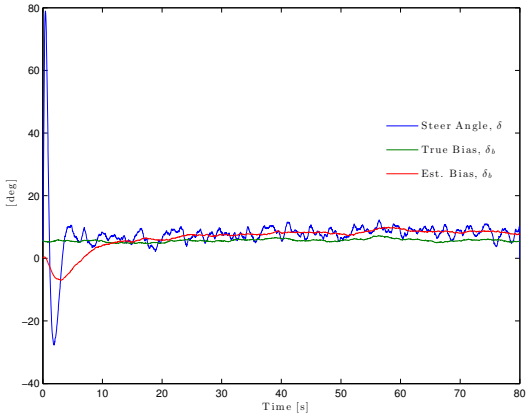

Figure 5: Steer Angle and Bias during Straight Line Tracking

Figure 6, below, shows the radar and heading angle bias estimations. As was done in [5], a rough estimate of the radar bias (r_b) is formulated by taking the difference between unbiased GPS-based velocity estimates and the biased radar estimate.

$$V_{GPS} \approx \frac{\sqrt{(E_{k+1} - E_k)^2 + (N_{k+1} - N_k)^2}}{T_s}$$
$$\Delta V_x = V_x^{radar} - V_{GPS}$$

This rough estimation creates noisy results for ΔV_x, but the bias should track the mean value of the radar error, as shown.

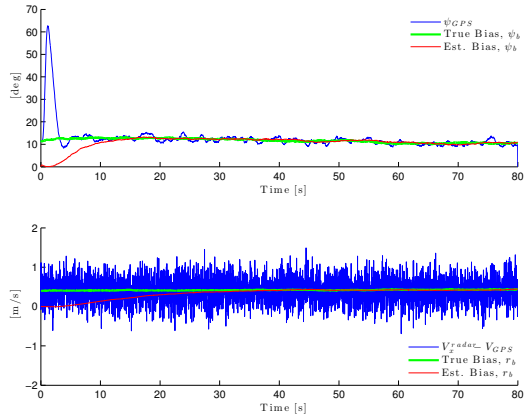

Figure 6: Heading and Radar Bias during Straight Line Tracking

In summary, the cascaded filters architecture enables the simultaneous estimation of the steer angle bias and the gyroscope bias, which would have created difficulty for a single filter. The estimators are able to converge to their true states quite well, although the transient performance can be improved quite a bit.

9.2. Unscented Kalman Filter Results

An 'aerial' view of the vehicle's trajectory is shown in Figure 7, together with a plot of the East estimation error of the Unscented Kalman Filter. The initial, larger error is present like before, however it is mitigated more quickly. The trajectory performance is very similar to the EKF case, however the East/North position estimation error appears larger for the UKF. This will be discussed in the next section (Section 9.3).

The UKF estimations of the four biases (radar, gyroscope, heading, and steer) are shown in Figure 8. Convergence of the radar bias is again the

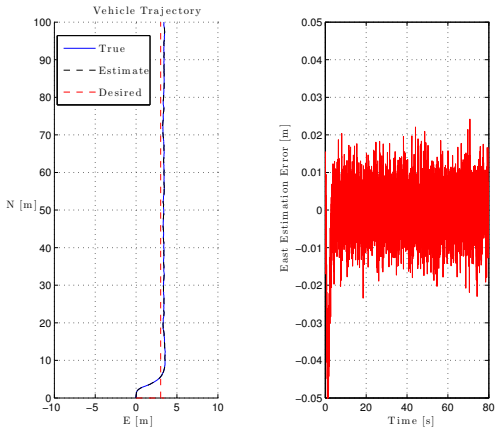

Figure 7: Straight Line Tracking & Position Error

slowest, but is happening approximately twice as fast as compared to the EKF radar bias estimation. The rest of the biases are estimated within a few seconds, which can be of critical importance during vehicle maneuvers or when a more complex control law is being used.

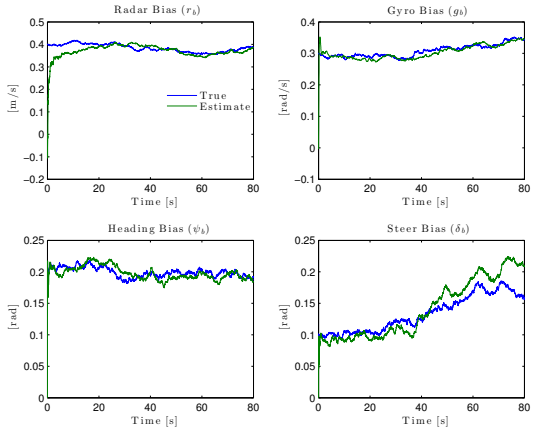

Figure 8: Bias Estimation during Straight Line Tracking

Figure 9 and Figure 10 (next page) show the gyroscope and radar measurements, respectively, together with the associated biases and estimation results.

Figure 11 (next page) shows the radar and heading angle bias estimations. Again, a rough estimate of the radar bias (r_b) is formulated by taking the difference between unbiased GPS-based velocity estimates and the biased radar estimate.

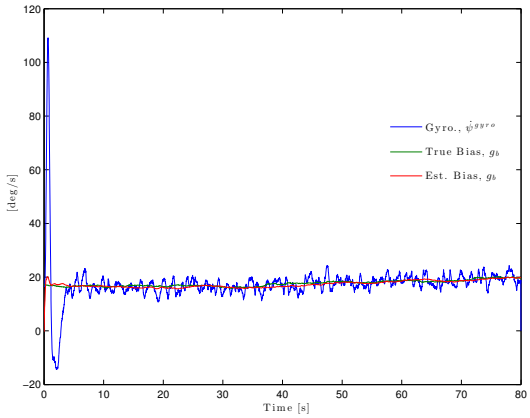

Figure 9: Gyroscope Measurements and Bias during Straight Line Tracking

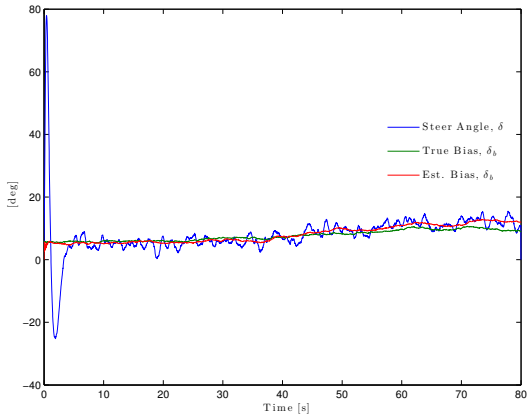

Figure 10: Steer Angle and Bias during Straight Line Tracking

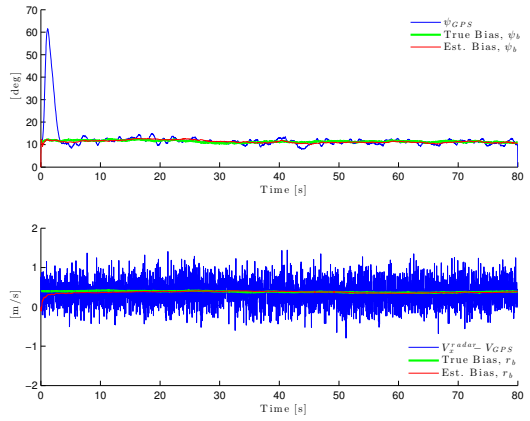

Figure 11: Heading and Radar Bias during Straight Line Tracking

9.3. EKF-UKF Comparison

In this section, the performance of the cascaded EKFs and cascaded UKFs is discussed. The following plots present a comparison of the absolute value of the estimation errors of the biases for each set of filers.

In Figure 12 and Figure 13 it is evident that the UKF filters are able to converge to the biases more quickly than the EKF filters, and remain very close to the true bias. Throughout the rest of the 80 second simulation, the UKF estimation error is either the same or below that of the EKF.

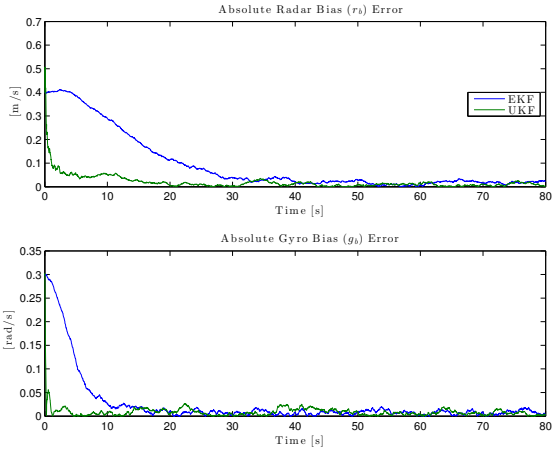

Figure 12: EKF-UKF Error Comparison

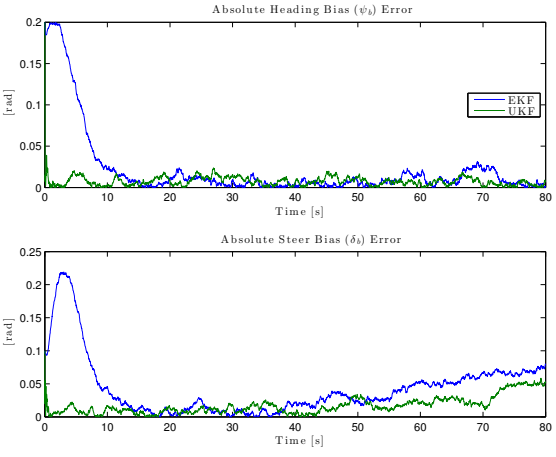

Figure 13: EKF-UKF Error Comparison

These results suggest that the cascaded Unscented Kalman Filters are indeed more appropriate for GPS/INS integration in systems with nonlinear dynamics. The faster and more accurate es-

timations of the UKF would enable the vehicle to cope with GPS outages without as much integration drift. Additionally, the biases would be more likely to be updated correctly if there are short spurts of GPS availability during a long GPS outage.

The main disadvantage of using the UKF is that it can become computationally expensive depending on the size of the system matrix. This is because the sigma vectors require the computation of the square root of the covariance matrix. The preferable method for computing this inverse with application to the UKF is by using the Cholesky decomposition. This is the method that was used in the paper. The UKF estimation required slightly more time than the EKF, although this could be partially due to differences in programming implementations.

One apparent issue with the estimation, however, is in the estimations of the East and North position states. The Extended Kalman Filter maintains a smaller estimation error than the UKF, especially in the North state.

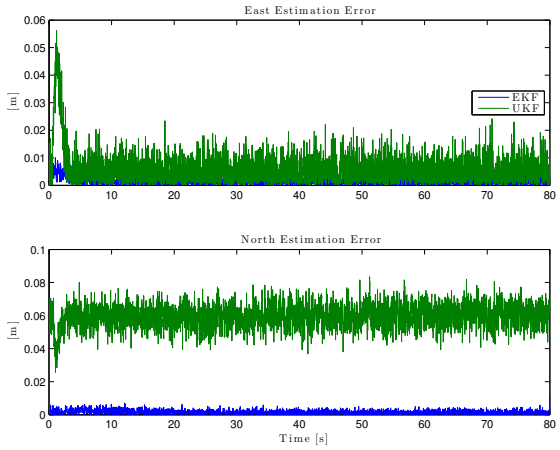

Figure 14: EKF-UKF Error Comparison

This could suggest that although the UKF is better for estimating the biases, the EKF might be more appropriate for estimating the other states. Further work needs to be done in order to test this hypothesis.

Alternately, it could be beneficial to merge the EKF and UKF algorithm for more accurate and robust estimation. The authors in [1] presented a 'hybrid' EKF/UKF algorithm for implementation in a Simultaneous Localization and Mapping (SLAM) algorithm. In their paper, the EKF is employed in the update phase, while the UKF is used during propagation for computing only the state and its covariance. EKF-based equations are then used to compute the cross-correlation terms during propagation.

By using an EKF/UKF 'hybrid' controller, it may be possible to take advantage of the quick convergence of the UKF filters to the four biases, and also benefit from the more precise convergence of the EKF to some of the other states. This is another interesting avenue for future work and research.

10. Conclusion

Using cascaded estimation filters to solve the GPS/INS integration problem for ground vehicles is advantageous in several ways, as shown in [5]. The authors in [5] divide the vehicle's model into two cascaded subsystems, and use two EKFs for estimation. The main disadvantage of the EKF is its requirement to linearize the system at every time step (using first-order Taylor linearization). A highly nonlinear system would require higher-order terms to represent its dynamics more accurately. There exist higher-order EKF algorithms, but these are computationally expensive and very difficult to implement in real-time.

A variant of the Kalman Filter, the UKF does not require linearization of the nonlinear system. Instead, it introduces a deterministic sampling of points to propagate through the nonlinear system in order to capture a more accurate mean and covariance for *any* nonlinearity [18].

The work in this paper shows that the cascaded systems approach can be improved by using two UKFs rather than two EKFs. It is shown through simulations that the UKF filters are able to estimate the INS biases faster than the EKF filters, and generally have smaller estimation errors throughout. A cascaded hybrid UKF/EKF filter is proposed as a possible further improvement to the work in this paper.

Bibliography

[1] Juan Andrade-Cetto, Teresa Vidal-Calleja, and Alberto Sanfeliu. Unscented transformation of vehicle states in slam. In *Robotics and Automation, 2005. ICRA 2005. Proceedings of the 2005 IEEE International Conference on*, pages 323–328. IEEE, 2005.

[2] M.M. Atia, A. Noureldin, and M. Korenberg. Gaussian process regression approach for bridging GPS outages in integrated navigation systems. *Electronics Letters*, 47(1):52–53, 2011.

[3] David M Bevly, J Christian Gerdes, and Bradford W Parkinson. A new yaw dynamic model for improved high speed control of a farm tractor. *Journal of dynamic systems, measurement, and control*, 124(4):659–667, 2002.

[4] David Mark Bevly. *High speed, dead reckoning, and towed implement control for automatically steered farm tractors using GPS*. PhD thesis, Stanford University, 2001.

[5] D.M. Bevly and B. Parkinson. Cascaded kalman filters for accurate estimation of multiple biases, dead-reckoning navigation, and full state feedback control of ground vehicles. *Control Systems Technology, IEEE Transactions on*, 15(2):199–208, 2007.

[6] J. Blanch, T. Walter, and P. Enge. Satellite navigation for aviation in 2025. *Proceedings of the IEEE*, 100(Special Centennial Issue):1821–1830, 2012.

[7] C. Boucher, A. Lahrech, and J.-C. Noyer. Non-linear filtering for land vehicle navigation with GPS outage. In *Systems, Man and Cybernetics, 2004 IEEE International Conference on*, volume 2, pages 1321–1325 vol.2, 2004.

[8] C. Boucher and J.-C. Noyer. A hybrid particle approach for GNSS applications with partial GPS outages. *Instrumentation and Measurement, IEEE Transactions on*, 59(3):498–505, 2010.

[9] Andrea Cesetti, Emanuele Frontoni, Adriano Mancini, Andrea Ascani, Primo Zingaretti, and Sauro Longhi. A visual global positioning system for unmanned aerial vehicles used in photogrammetric applications. *Journal of Intelligent and Robotic Systems*, 61(1-4):157–168, 2011.

[10] A. Cole, Jinling Wang, C. Rizos, and A.G. Dempster. Bridging GPS outages in the agricultural environment using virtualite measurements. In *Position, Location and Navigation Symposium, 2008 IEEE/ION*, pages 497–504, 2008.

[11] M. El-Diasty and S. Pagiatakis. An efficient INS/GPS impulse response model for bridging GPS outages. In *Science and Technology for Humanity (TIC-STH), 2009 IEEE Toronto International Conference*, pages 328–333, 2009.

[12] Jacques Georgy, Aboelmagd Noureldin, Michael J Korenberg, and Mohamed M Bayoumi. Low-cost three-dimensional navigation solution for RISS/GPS integration using mixture particle filter. *Vehicular Technology, IEEE Transactions on*, 59(2):599–615, 2010.

[13] M. Ilyas, Yunchun Yang, Qiu Shi Qian, and Ren Zhang. Low-cost IMU/odometer/GPS integrated navigation aided with two antennae heading measurement for land vehicle application. In *Control and Decision Conference (CCDC), 2013 25th Chinese*, pages 4521–4526, 2013.

[14] Simon J Julier and Jeffrey K Uhlmann. New extension of the kalman filter to nonlinear systems. In *AeroSense'97*, pages 182–193. International Society for Optics and Photonics, 1997.

[15] Tak Kit Lau, Yun-Hui Liu, and Kai Wun Lin. Inertial-based localization for unmanned helicopters against GNSS outage. *Aerospace and Electronic Systems, IEEE Transactions on*, 49(3):1932–1949, 2013.

[16] Chong Shen, Xiyuan Chen, Wei-bin Zhang, Masayoshi Tomizuka, Yuan Xu, and Kuanlin Chiu. Novel hybrid of strong tracking kalman filter and wavelet neural network for GPS/INS during GPS outages. *Measurement*, 46(10):3847 – 3854, 2013.

[17] Hindupur V Sudarshan. *Seamless Sky*. Ashgate Publishing, Ltd., 2003.

[18] Eric A Wan and Rudolph Van Der Merwe. The unscented kalman filter for nonlinear estimation. In *Adaptive Systems for Signal Processing, Communications, and Control Symposium 2000. AS-SPCC. The IEEE 2000*, pages 153–158. IEEE, 2000.

[19] J. H Wang and Y. Gao. Land vehicle dynamics-aided inertial navigation. *Aerospace and Electronic Systems, IEEE Transactions on*, 46(4):1638–1653, 2010.

[20] Jinling Wang, Matthew Garratt, Andrew Lambert, Jack Jianguo Wang, S Han, and David Sinclair. Integration of GPS/INS/vision sensors to navigate unmanned aerial vehicles. *IAPRSSIS*, 37(B1):963–9, 2008.

[21] R. Wong, Sheng Hu, F. Cabrera-Mora, Jizhong Xiao, and Jindong Tan. A distributed algorithm for mobile robot localization and mapping in wireless sensor networks. In *Information and Automation, 2008. ICIA 2008. International Conference on*, pages 560–566, 2008.